J. Water Environ. Nanotechnol., 3(4): 321-336 Autumn 2018

ORIGINAL RESEARCH PAPER

Fe_3O_4/AC nanocomposite as a novel nano adsorbent for effective removal of cationic dye: Process optimization based on Taguchi design method, kinetics, equilibrium and thermodynamics

Maryam Ghasemi[1,*], Somaye Mashhadi[1], Javad Azimi-Amin[2]

[1] *Young Researchers and Elite Club, Arak Branch, Islamic Azad University, Arak, Iran*
[2] *Department of Agriculture, University of Mehrgan, Mahalat, Iran*

Received: 2018-07-31 Accepted: 2018-09-13 Published: 2018-10-15

ABSTRACT
In this study, we have synthesized a new Fe_3O_4/AC nanocomposite using low-cost adsorbent by microwave assisted in situ co-precipitation technique that was used as an effective adsorbent for the removal of methylene blue (MB) using the Taguchi design method as an optimization strategy. The optimum parameters are pH 7, Fe_3O_4/AC nanocomposite dose 0.03 g, contact time 30 min, initial concentration of MB 25 mg/L and temperature 298 K. The obtained results of ANOVA show that their percent contribution in descending order is pH (66.81%) > adsorbent dose (25.54%) > temperature (4.83%) > initial MB concentration (1.23%) > contact time (0.32%). The kinetic data were fitted to the pseudo-first-order, pseudo-second-order and intra-particle diffusion models and adsorption of MB dye followed pseudo-second-order kinetics. The obtained values of regression coefficient for Langmuir (0.98), Freundlich (0.93) and Dubinin–Radushkevich (0.94) showed that adsorption process fits to the Langmuir isotherm and the maximum adsorption capacity is 384.6 mg/g. Moreover, the thermodynamics studies suggested the spontaneous nature of the adsorption process.

Keywords: *Magnetite Nanoparticles, Methylene Blue, Microwave-Induced, Nanocomposite, Taguchi Method*

How to cite this article
Ghasemi M, Mashhadi S, Azimi-Amin J. Fe_3O_4/AC nanocomposite as a novel nano adsorbent for effective removal of cationic dye: Process optimization based on Taguchi design method, kinetics, equilibrium and thermodynamics. J. Water Environ. Nanotechnol., 2018; 3(4): 321-336. DOI: 10.22090/jwent.2018.04.005

INTRODUCTION

High quantities of pollutants such as synthetic dyes, metal ions, phenols, and fertilizers discharge into surface and groundwater. The productive sources of these pollutants are mining, chemical manufacturing, metallurgical, tannery, battery manufacturing industries, textile, leather, paper, and plastics industries etc [1, 2]. Wastewaters containing dyes, even at very low concentration, can disturb the ecosystem both the environment and the human. Colored wastewater causes a reduction of sunlight penetration and affects the photosynthetic activity of aquatic organisms. In addition, these kinds of pollutants are toxic, carcinogenic, mutagenic, or teratogenic for various microbiological and fish species [3]. Methylene blue (MB), as one of the commonly known dye, belongs to a thiazine cationic dye used in various applications like coloring paper cotton, wools and temporary hair colorant [4, 5]. Therefore, it is necessary to eliminate the risk of trapping the colors in wastewater and environmental hazards [6].

Various processes such as electrochemical techniques, membrane separation, ion exchange, adsorption, photo-catalysis, and photo-oxidation had used to eliminate dyes from the dyeing wastewater before its discharge to freshwater [7-9]. Among these processes, adsorption is the most widely used process due to high efficiency to treat dyes in more concentrated forms and low cost of the application and ease of operation [10, 11]. Various

* Corresponding Author Email: *maryam_ghasemi6282@yahoo.com*

kinds of adsorbents have been used to remove MB dye from wastewater such as peanut hulls [12], walnut wood [5], Albizia lebbeck seed pods [13], peanut sticks wood [7], almond shell [14], corn straw [15], Harmal seeds residue [16] and papaya leaves [17]. In order to improve the reactivity and adsorption capacity of adsorbent for the removal of dye, various modification materials and methods have been used; such as cationic surfactants [18], magnetic particles [19], metal oxides [20], chemical activating agents [21], organic reagents [22] and amino functionalities [23]. Among these materials, magnetic nanoparticles have been considered to be an ideal candidate for modification of surface because of their unique large surface areas, well-defined pore sizes, high pore volume, and easy separation by applying an external magnetic field [24-26]. Therefore, studies on the synthesis of magnetic nanoparticles have increased during the past decade using a variety of techniques such as hydrothermal, co-precipitation, sol-gel, chemical vapor deposition, microwave assisted, ultrasonic irradiation and anodic arc plasma [27]. Microwave radiations possess both electrical and magnetic properties. Microwave radiation is able to interact directly with the particles inside the material and changes electromagnetic energy into heat transfer inside the dielectric materials. Using Microwave radiation has the advantages such as lower activation temperature, immediate startup and shutdown, smaller steps, improved safety and improved efficiency [28. 29]. Further, Microwave radiation gives nanoparticles with smaller particle size, narrow size distribution, and high purity [30]. Thus, these features make the microwave-assisted process as a superior method over the others as magnetic stirring applied. *Myrtus Communis* is a wild plant and belongs to the family of Myrtaceae that grows rapidly in different regions. Different parts of this plant were used in the food and medicine industries, such as leaves, white star-like delicate flowers and dark-blue berry fruit containing the seeds [31]. Even though there are studies on the removal of the dye with magnetic nanoparticles covered activated carbon (AC), there is no any study for the removal of MB by using AC obtained from *Myrtus Communis*.

In order to find out the optimum removal efficiency in a batch system, it is necessary to identify effective parameters such as pH, contact time, dose, initial concentration, temperature, etc. Taguchi method, as a statistical tool and useful design of experimental approach, is a multivariate optimization method that reduces the cost of experiments and time of experimental investigation and presents more information about the whole process [32, 33]. However, there are few studies reported in the literature regarding the utilization of Taguchi statistical method in the field of dye removal from aqueous solutions and wastewaters.

In the present research, Fe_3O_4/AC nanocomposite was successfully synthesized by microwave assisted in situ co-precipitation technique at room temperature. The Taguchi statistical method with L_{27} orthogonal array was applied to find the optimum parameters for MB removal using new magnetite activated carbon adsorbent. The analysis of variance (ANOVA) and signal-to-noise (S/N) ratio techniques were used for identification of the most effective parameters on the removal efficiency of MB dye from aqueous solutions using magnetite activated carbon adsorbent. In addition, adsorption isotherm, kinetic and thermodynamic studies were performed to find the adsorption mechanism and efficiency of Fe_3O_4/AC nanocomposite.

MATERIALS AND METHODS

Reagents

All chemicals and reagents used in this study were of analytical reagent grade. $FeCl_3.6H_2O$, $FeCl_2.4H_2O$, H_2SO_4, $NaHCO_3$, NaOH, and MB dye were purchased from Merck. The Chemical structure of MB (chemical formula of $C_{16}H_{18}N_3SCl$, λ_{max} of 663 nm) was shown in Fig. 1. The stock solution (100 mg/L) of MB was prepared by dissolving 10 mg of MB dye in 100 ml deionized water and was diluted with deionized water to the desired MB concentrations.

Preparation of Myrtus Communis activated carbon

Myrtus Communis leaves (Raw M) were washed with tap water and then boiled in deionized water for 2 h to remove the water-soluble phenolic and other organic compounds. Subsequently, they were

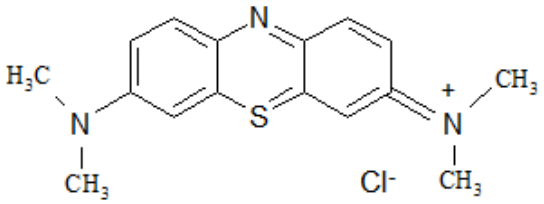

Fig. 1. Physical properties and molecular structure of Methylene blue (MB)

washed several times with deionized water and dried at 80 °C for 12 h. The dried samples were crushed and sieved (100–120 mesh). The activated carbon was prepared according to Demirbas. et al [34]: 50 g Sieved sample was soaked in the concentrated H_2SO_4 solution and was activated in the air oven at 105 °C for 24 h. In order to remove the free acid, the mixture was washed with distilled water and then immersed in a 1% $NaHCO_3$ solution. The carbonized material was placed in a ceramic crucible and activated in the furnace at 700 °C with a retention time of 3 h. Finally, the activated carbon was filtered and washed with deionized water and dried in the air oven at 105 °C.

Preparation of Fe_3O_4/AC

Fe_3O_4/AC nanocomposite was prepared by co-precipitation of Fe(II) and Fe(III) ions in aqueous solution by NaOH using microwave assisted.

$$NaOH \rightarrow Na^+ + OH^-$$
$$Fe^{2+} + 2Fe^{3+} + 8OH^- \rightarrow Fe_3O_4 + 4H_2O$$

At first, the activated carbon was added to a 100 mL solution containing $FeCl_3$.6H2O, $FeCl_2.4H_2O$ (molar ratio of 2:1), at room temperature and stirred for 10 min. Then, 50 ml of NaOH solution (0.5 mol/L) was added drop-wise to raise the suspension pH to around 9. The prepared sorbent was heated under microwave irradiation with an output power of 500 W for 20 min. The prepared nanocomposite was washed with deionized water until the pH of the solution become neutral and then dried in an oven at 80°C for 12 h.

Instruments

The morphology of the *Myrtus Communis* leaves, activated carbon and Fe_3O_4/AC nanocomposite was examined using the field emission scanning electron microscope (FESEM) (Hitachi-S4160, Japan) under an acceleration voltage of 20 kV. X-ray diffraction studies of Fe_3O_4/AC nanocomposite sample was done by using X-ray diffractometer (APD 2000, Italy). The organic functional groups of *Myrtus Communis* leaves activated carbon and Fe_3O_4/AC nanocomposite was determined by FTIR spectroscopy (Shimadzu-8400S, Japan) in the wavelength of 4000–500 cm^{-1}. The pH of MB dye solution was adjusted by using 0.1 mol/L H_2SO_4 and NaOH and measured with a pH meter (Metrohm-827, USA). The samples were dried in program controller JEIO TECH (CF-02G KOREA). Also, a microwave oven (MOLINEX, MVV 200130 2450 MHZ) was used for synthesized of the Fe_3O_4/AC nanocomposite. The residual MB concentration in the aqueous solution before and after the adsorption process was measured by a UV/Vis spectrophotometer (Perkin-Elmar-lambada25).

MB adsorption experiments

In this research, the batch experiments were studied by Taguchi statistical method. The percentage MB removal was estimated for different experimental conditions including pH, adsorbent dose, contact time, initial dye concentration and temperature. The amount of MB adsorbed per unit mass of Fe_3O_4/AC nanocomposite (adsorption capacity) was calculated using Eq. (1):

$$q_e = \frac{(C_o - C_e)V}{m} \quad (1)$$

The percentage MB removal was calculated using the following equation:

$$\%\,Re = \frac{(C_o - C_e)}{C_o} \times 100 \quad (2)$$

in these formulas, C_o (mg/L) and C_e (mg/L) are the concentration of MB dye before and after adsorption experiments, respectively. q_e (mg/g) is the adsorption capacity of MB dye onto Fe_3O_4/AC nanocomposite, V (L) is the solution volume of MB dye, and m (g) is the amount of Fe_3O_4/AC nanocomposite adsorbent.

Taguchi method

In this research, five controllable factors including pH, adsorbent dose, contact time, initial dye concentration and temperature were designed in three levels as shown in Table 1. A standard

Table 1. Factors and their levels for design of experiments

Factor	Unit	Level		
		1	2	3
pH	--	3	5	7
Adsorbent dose	g	0.005	0.01	0.03
Contact time	min	1	30	60
Initial dye concentration	mg/L	25	45	65
Temperature	K	298	318	338

L_{27} (3^5) orthogonal array design (OAD) was used to determine the optimum experimental conditions for maximum removal of MB dye and the designed experimental runs are given in Table 2. The signal/noise (S/N) ratio is used to measure the deviation of the output characterization from the desired values [35, 36]. In this method, the quality characteristics of data are categorized into "the larger is the better", "the normal is the best", and "the smaller is the better" types. According to the goal of this research, "the larger is the better" was selected to define the optimum conditions. The S/N ratio is defined as [33]:

$$\frac{S}{N} = -10\log\frac{(1/y_1^2 + 1/y_2^2 + ... + 1/y_n^2)}{n} \quad (3)$$

In this formula, n is the replication number of the experiment and y_i is the experimental response. After calculating values of S/N ratio for each experimental test, in order to obtain the optimum conditions of the removal process, the highest value of S/N ratio was selected as the optimum condition for removal process [37].

RESULTS AND DISCUSSION

Characterization

Fig. 2 shows the FESEM images of *Myrtus Communis* leaves, activated carbon and Fe_3O_4/AC nanocomposite at different magnification, respectively. As seen from the image, the surface of Raw M leaf is soft, smooth and without any porosity. Activation process creates some changes on the surface of Raw M. These changes including a porous and rough surface with deep pores that is favorable for removal dye on the sorbent. According to Fig. 2(c), the Fe_3O_4 nanoparticles cover the surface of activated carbon with good homogeneity in shape and size. As seen the Fig. 2c, microwave irradiation provided nanoparticles with higher purity and uniformly in a shorter time. These observations are similar to the morphology of nanoparticles by Osouli-Bostanabad et al. and Hernández-Hernández et al. [27, 28].

The XRD pattern of Fe_3O_4/AC nanocomposite (Fig. 3) showed the diffraction peaks at 2θ= 29.4, 35.4, 43.2, 52.9, 57.2 and 62.6. The existence of these peaks in Fe_3O_4/AC nanocomposite confirms the incorporation and uniform distribution of Fe_3O_4 nanoparticles in the nanocomposite. Furthermore, the narrow sharp peaks indicate that the Fe_3O_4 nanoparticles are well crystallized.

The FTIR spectrums of Raw M activated carbon and Fe_3O_4/AC nanocomposite are presented in Fig. 4, respectively. The broad adsorption band at 3463 cm^{-1} is related to the bonded –OH stretching

Table 2. L_{27} orthogonal arrays

Expt. no.	pH	Adsorbent dose (g)	Contact time (min)	Initial dye concentration (mg/L)	Temperature (K)	%Re	S/N
1	3	0.005	1	25	298	83.5	38.43
2	3	0.005	1	25	318	82.8	38.36
3	3	0.005	1	25	338	80.6	38.12
4	3	0.01	30	45	298	85.1	38.59
5	3	0.01	30	45	318	84.9	38.57
6	3	0.01	30	45	338	83.4	38.42
7	3	0.03	60	65	298	87.3	38.82
8	3	0.03	60	65	318	85.8	38.66
9	3	0.03	60	65	338	84.2	38.50
10	5	0.005	30	65	298	88.7	38.95
11	5	0.005	30	65	318	88.2	38.90
12	5	0.005	30	65	338	87.9	38.87
13	5	0.01	60	25	298	94.2	39.48
14	5	0.01	60	25	318	91.1	39.19
15	5	0.01	60	25	338	89.7	39.05
16	5	0.03	1	45	298	95.01	39.55
17	5	0.03	1	45	318	94.8	39.53
18	5	0.03	1	45	338	93.1	39.37
19	7	0.005	60	45	298	89.6	39.04
20	7	0.005	60	45	318	88.3	38.19
21	7	0.005	60	45	338	87.9	38.87
22	7	0.01	1	65	298	92.2	39.29
23	7	0.01	1	65	318	91.1	39.19
24	7	0.01	1	65	338	90.2	39.10
25	7	0.03	30	25	298	96.2	39.66
26	7	0.03	30	25	318	95.2	39.57
27	7	0.03	30	25	338	94.1	39.47

vibrations of OH and COOH functionalities [38]. The band at 2360 cm^{-1} is corresponding to the carboxyl group. The band at approximately 1596 cm^{-1} is attributed to the C=C vibrations [39]. The peaks at 1157-1118 cm^{-1} indicate the C-O-C groups [40]. After activation process, several changes or shifts happened in the spectrum of activated carbon. The new peak at 2923 cm^{-1} is related to aldehydic C-H and alkane C-H stretching vibrations [41]. As can be seen in Fig. 4(c), the band at 667 cm^{-1} (belong to the Fe_3O_4) is confirmation of the successful bonding of Fe coupling onto the Fe_3O_4/AC nanocomposite surface [42].

Taguchi results and effects of parameters

Results of experiments designed by the Taguchi method and the calculated S/N (signal to noise) ratio for each experiment are presented in Table 2. The obtained results of Table 2 show that the percentage of MB removal varied from 80.6% to 96.2%, and S/N ratios from 38.12 to 39.6. The results are given in Table 3 and Fig. 5 indicates that the best level for each controllable factor is level 3 for pH, level 3 for adsorbent dose, level 2 for contact time, level 1 for initial dye concentration and level 1 for temperature. On the other hand, the best levels for the MB removal are pH 7, Fe_3O_4/AC

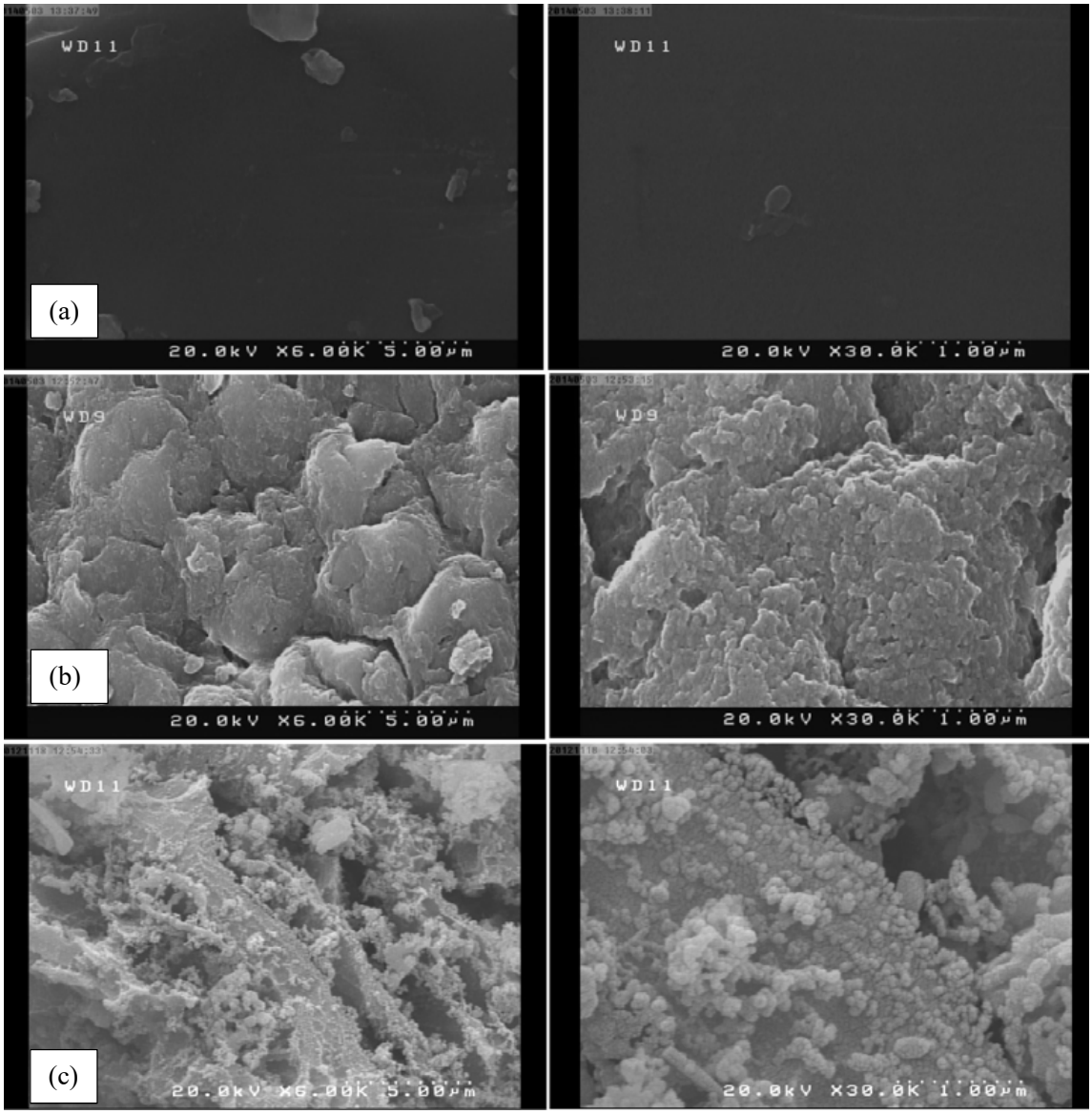

Fig. 2. FESEM image of (a) Raw M (b) activated carbon and (c) Fe_3O_4/AC nanocomposite at different magnification

nanocomposite dose 0.03 g, contact time 30 min, initial MB concentration 25 mg/L and temperature 298 K. It can be observed from the above results that the order of importance of controllable factors for the removal of MB using Fe_3O_4/AC nanocomposite is pH, adsorbent dose, temperature, initial dye concentration and contact time, respectively. It shows that the pH factor is the most significant controllable factor of MB removal. Another ability of the Taguchi method is to predict the removal percent of MB dye in optimum condition. The amount predicted by the Taguchi method is 98.8% that is very close to this achieved experimentally in the same condition with the closeness of 98.0%.

Effect of pH

The pH of solution is one of the important parameters for the removal of dyes and it can effect on surface charge of adsorbent [43]. According to the above results, the highest S/N ratio was achieved at the highest level of pH. On the other hands, the S/N values increases by increasing pH from 3 to 7 and maximum S/N occurred at pH 7. At low pH and acidic conditions of the solution, the dimethylamine groups in MB ions are protonated. Moreover, the surface of Fe_3O_4/AC nanocomposite is surrounded by the hydrogen ions that compete with MB ions for interaction with the active sites of the adsorbent. Therefore, there is a lower removal

Table 3. Response table of S/N ratios and contribution of each controllable factor

Level	pH	Adsorbent dose	Contact time	Initial dye concentration	Temperature
1	38.50	38.72	39.00	39.04	39.09
2	39.22	38.99	39.01	38.99	38.99
3	39.24	39.24	38.95	38.93	38.87
Delta	0.74	0.52	0.05	0.11	0.23
Rank	1	2	5	4	3

Table 4. Results of the analysis of variance (ANOVA)

Factor	Degree of freedom	Sum of Squares	Mean Squares	F value	*p*-value	Percent contribution
pH	2	3.157	1.578	429.75	0.000	66.81
Adsorbent dose	2	1.207	0.603	164.33	0.000	25.54
Contact time	2	0.015	0.007	2.08	0.157	0.32
Initial dye concentration	2	0.058	0.029	7.97	0.004	1.23
Temperature	2	0.228	0.114	31.09	0.000	4.83
Residual	16	0.058	0.003			
Total	26	4.725				

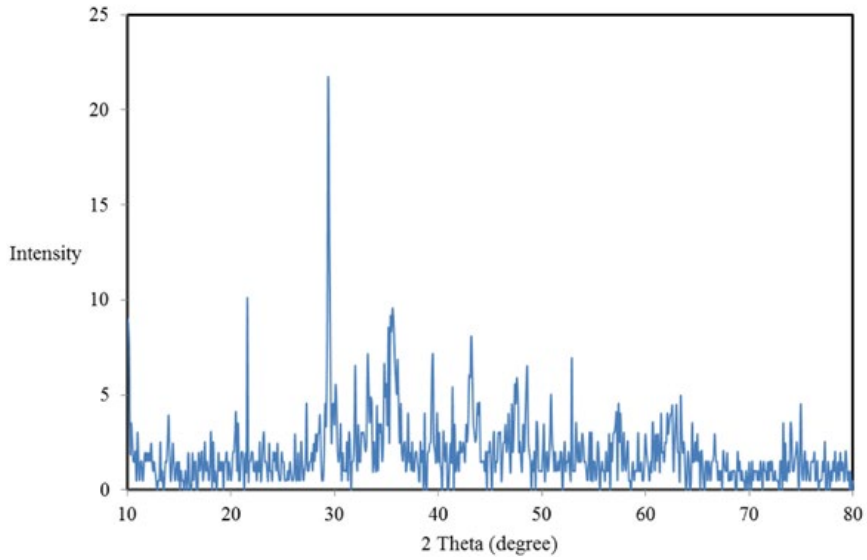

Fig. 3. XRD pattern of Fe_3O_4/AC nanocomposite

at lower pH values and adsorption process is weak due to the competition of H_3O^+ and MB cations. At higher pH and neutral or basic conditions of the solution, hydrogen bonding and electrostatic interactions between MB ions and functional groups of Fe_3O_4/AC nanocomposite during the adsorption process cause an efficient removal of MB ions from aqueous solution (Scheme 1) [44, 45]. There are abundant of hydroxyl and groups on Fe_3O_4/AC nanocomposite surface. As can be seen in Scheme 1, the adsorption process occurred through hydrogen bonding between the hydroxyl groups on the Fe_3O_4/AC nanocomposite and the electronegative groups on the MB dye molecule. Furthermore, the presence negatively charged functional groups on Fe_3O_4/AC nanocomposite (such as O^- and COO^-) and their interaction with the electronegative groups on the MB cause an efficient removal of MB ions.

Effect of adsorbent dose

The adsorbent dose is an important parameter for the removal of dyes due to presence vacant active sites and pores on the surface of adsorbent [46]. Experiments were designed with 3 levels of adsorbent dose from 0.005 to 0.03 g. The

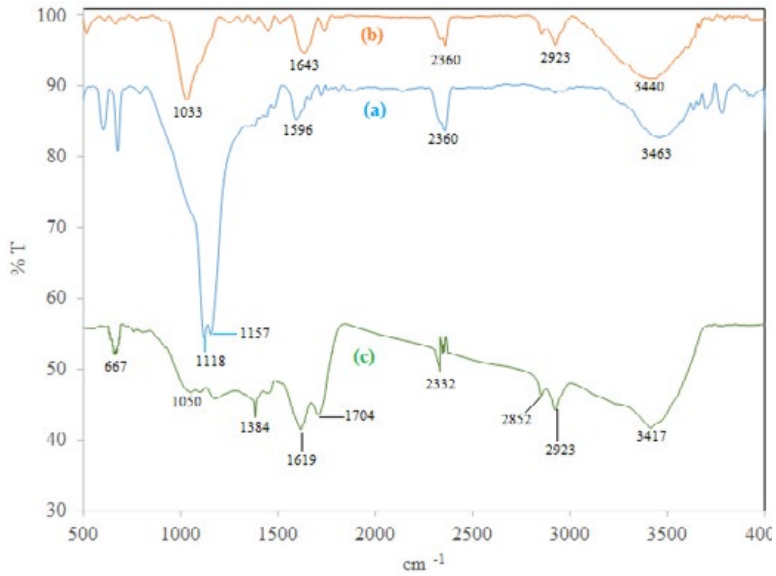

Fig. 4. FTIR spectrum of (a) Raw M (b) activated carbon and (c) Fe_3O_4/AC nanocomposite

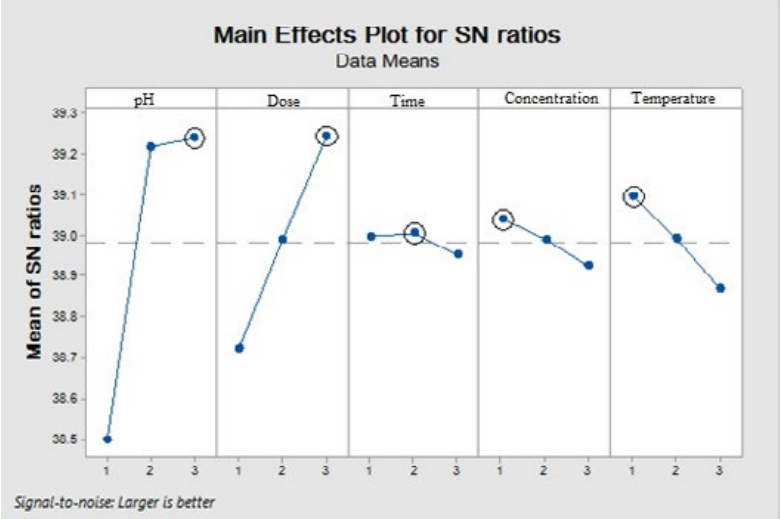

Fig. 5. The variation of S/N ratio of different factors

highest S/N ratio was achieved at the highest level of adsorbent dose and maximum removal occurred at an adsorbent dose of 0.03 g. As can be seen from Fig. 4, the removal efficiency of MB increased by increasing adsorbent dose because of raising number vacant sites toward dye molecule at constant dye concentration. On the other hand, by increasing the amount of adsorbent in aqueous solution, the surface area increased, and consequently, the number of active sites available for adsorption process increased. The obtained result from this study is in accordance with the similar studies [5, 47, 48].

Effect of contact time

According to obtained results from Table 3, the highest S/N ratio was achieved at the second level of contact time. On the other words, the maximum percentage MB removal occurred at contact time 30 min. It shows that the variation of S/N ratios of contact time is the smallest and contact time is the least important variable influencing the dye removal. At the beginning of the adsorption process, the fast adsorption occurs on the surface of Fe_3O_4/AC nanocomposite. This may be due to the availability of active sites and functional groups on the surface and large surface area of adsorbent. By passing time, reducing vacant sites and creating repulsive forces between the dye molecules on the solid and bulk phase might be responsible for decreasing the MB removal [49, 50].

Effect of initial concentration

The effect of MB initial concentration in the range of 25 to 65 mg/L was investigated and the highest S/N ratio was achieved at the first level of initial concentration. On the other hands, the S/N value for MB concentration decreases from 39.04 to 38.93 by increasing initial concentration from 25 to 65 mg/L and maximum S/N occurred at MB initial concentration of 25 mg/L. According to these results, the removal efficiency of dye decreases with the increasing MB initial concentration. This phenomenon might be due to the saturation of the surface of Fe_3O_4/AC nanocomposite adsorbent or possible repulsive force between adsorbed layers on the surface of adsorbent and remaining bulk dye molecules [51].

Effect of temperature

Experiments of related to temperature were designed with three levels of temperature from 298 to 338 K and the highest S/N ratio was achieved at the lowest level of temperature. In the other hands, after the temperature of 298 K of the solution, the removal of dye decreased. The continuous decrease in the removal efficiency of MB dye may be due to the weak attraction between MB and adsorbent

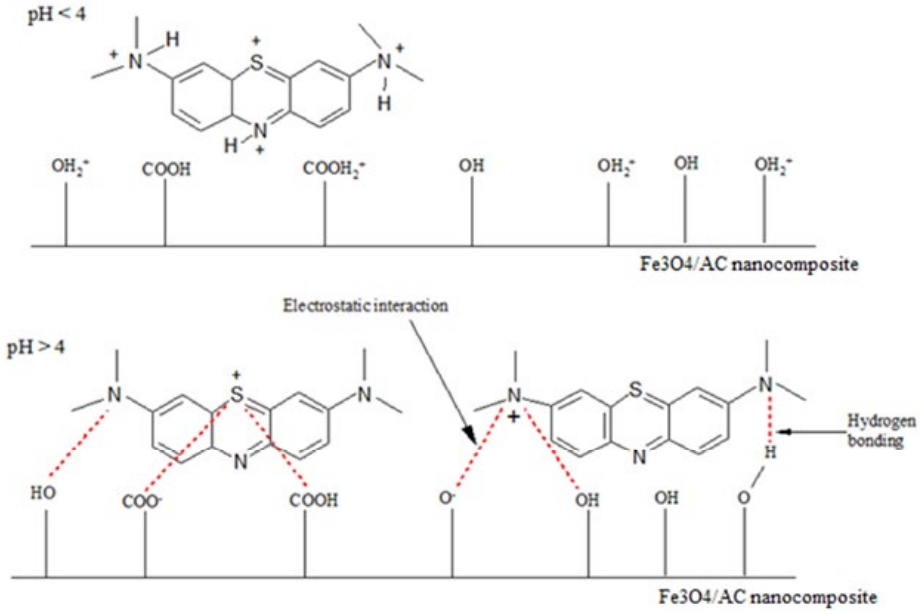

Scheme 1. A plausible mechanism for the sorption of MB onto Fe_3O_4/AC nanocomposite

[47] and or increasing temperature of solution leads to creation the tendency of dye molecules to escape from the solid phase to bulk phase [52].

Analysis of variance (ANOVA)

In order to investigate significant parameters and percent contribution of each controllable factor to the response, the analysis of variance (ANOVA) was used. According to the results of Table 4, the degree of freedom (DOF) for each factor was 2 with a total DOF of 26. A *p*-value less than 0.05 indicate that the estimated model is significant [53]. The obtained results of this indicator show that pH, adsorbent dose, initial dye concentration, and temperature are significant parameters and contact time is an insignificant parameter. Based on the ANOVA results, the rank order of the percentage contributions of each factor is as follows: (1) the pH of solution (66.81%), (2) adsorbent dose (25.54%), (3) temperature (4.83%), (4) initial dye concentration (1.23%) and (5) contact time (0.32%). According to Table 4, the parameter of contact time is the least important variable influencing the dye removal. Similar reports have been observed in other studies [33, 35]. The obtained results of Tables 3 and 4 show that the order of influence of controllable factors for the removal is same by comparison of the highest S/N ratio and percentage contributions of ANOVA.

Kinetic study

In this part of the study, the adsorption kinetics of MB onto Fe_3O_4/AC nanocomposite were investigated by using the pseudo-first-order, the pseudo-second-order, and the intra-particle diffusion model.

The pseudo-first-order [54] model is based on the rate of adsorbate seizing the adsorption sites is proportional to the number of untaken adsorption sites. This model is:

$$\log(q_e - q_t) = \log q_e - \frac{k_1}{2.303} t \quad (4)$$

In this formula, q_t and q_e are the amount of MB (mg/g) adsorbed at time t and equilibrium, respectively, and k_1 (1/min) is the rate constant of the pseudo-first-order equation of the adsorption. The values of constants (q_e and k_1) are determined by plotting log (q_e–q_t) versus t.

The pseudo-second-order [43] model is based on the sorbent adsorbed the adsorbate chemically. This model is:

$$\frac{t}{q_t} = \frac{1}{k_2 q_e^2} + \frac{t}{q_e} \quad (5)$$

In this formula, q_t and q_e are the amount of MB (mg/g) adsorbed at time t and equilibrium, respectively, and k_2 (g/mg.min) is the rate constant of the pseudo-second-order equation of the adsorption. The values of constants (q_e and k_2) are determined by plotting t/q_t versus t.

The intra-particle diffusion [52] model is:

$$q_t = k_i t^{1/2} + y \quad (6)$$

In this formula, k_i is the initial rate of intra-particle diffusion (mg/g.min $^{1/2}$), and y (mg/g) is the intercept. The values of constants (k_i and y) are determined by plotting q_t versus $t^{1/2}$.

The best model of kinetic adsorption is confirmed by correlation coefficients (R^2). Moreover, the applicability of the best kinetic model to describe the adsorption process is confirmed by nonlinear Chi-square test ($\chi 2$) and average relative error (ARE) [55]. These error functions are:

$$\chi^2 = \sum_{i=1}^{N} \frac{(q_{e,exp} - q_{e,cal})^2}{q_{e,exp}} \quad (7)$$

$$ARE = \frac{100}{N} \sum_{i=1}^{N} \left| \frac{q_{e,exp} - q_{e,cal}}{q_{e,exp}} \right|_i \quad (8)$$

In these formulas, $q_{e,exp}$ is the observation value from the batch experiment in an equilibrium state, $q_{e,cal}$ is calculated value from the kinetic equations (equations 4-6) and N is the number of observations in the experimental kinetic.

The result of the effect of contact time on the adsorption of MB onto Fe_3O_4/AC nanocomposite is shown in Fig. 6a. The plots of pseudo-first-order and pseudo-second-order are shown in Fig. 6(b and c) and obtained results from these plots are listed in Table 5. The results show that the value of $q_{e,cal}$ (222.2 mg/g) is near to value of $q_{e,exp}$ (223.9 mg/g) for the pseudo-second-order model. Moreover, the value of the correlation coefficient is very high and close to unity. In addition, the χ^2 and ARE values for the pseudo-second-order are 0.012 and 0.084, which are lower than those for the pseudo-first-order model. According to the above results, the pseudo-second-order model best fit the adsorption kinetic of MB dye onto the Fe_3O_4/AC nanocomposite and this indicates that the adsorption process was enhanced by chemisorption [5, 52].

In a solid/liquid adsorption process, solute diffusion into sorbent is done by external mass transfer, intra-particle diffusion, or both of them [56]. Therefore, the intra-particle diffusion model was used to analyze the mechanism of MB adsorption. As shown in Fig. 6d, the plot of q_t versus $t^{1/2}$ does not pass through the origin and it separated into two linear regions. This kind of plot shows that the adsorption process is multiple stages. Therefore, external mass transfer and intra-particle diffusion control the adsorption process and intra-particle diffusion is not the sole rate-controlling step.

Table 5. The adsorption kinetics of MB dye

Model	Parameter	Value
	$q_{e,exp}$ (mg/g)	223.9
Pseudo-first-order	$q_{e,cal}$ (mg/g)	23.52
	k_1 (1/min)	0.057
	R^2	0.631
	$\chi 2$	179.3
	ARE	9.94
Pseudo-second-order	$q_{e,cal}$ (mg/g)	222.2
	k_2 (g/mg.min)	0.020
	R^2	0.999
	$\chi 2$	0.012
	ARE	0.084
Intra-particle diffusion	k_{i1} (mg/g.min$^{1/2}$)	2.512
	y (mg/g)	206.78
	R^2	0.985
	k_{i2} (mg/g.min$^{1/2}$)	0.432
	y (mg/g)	219.12
	R^2	0.943

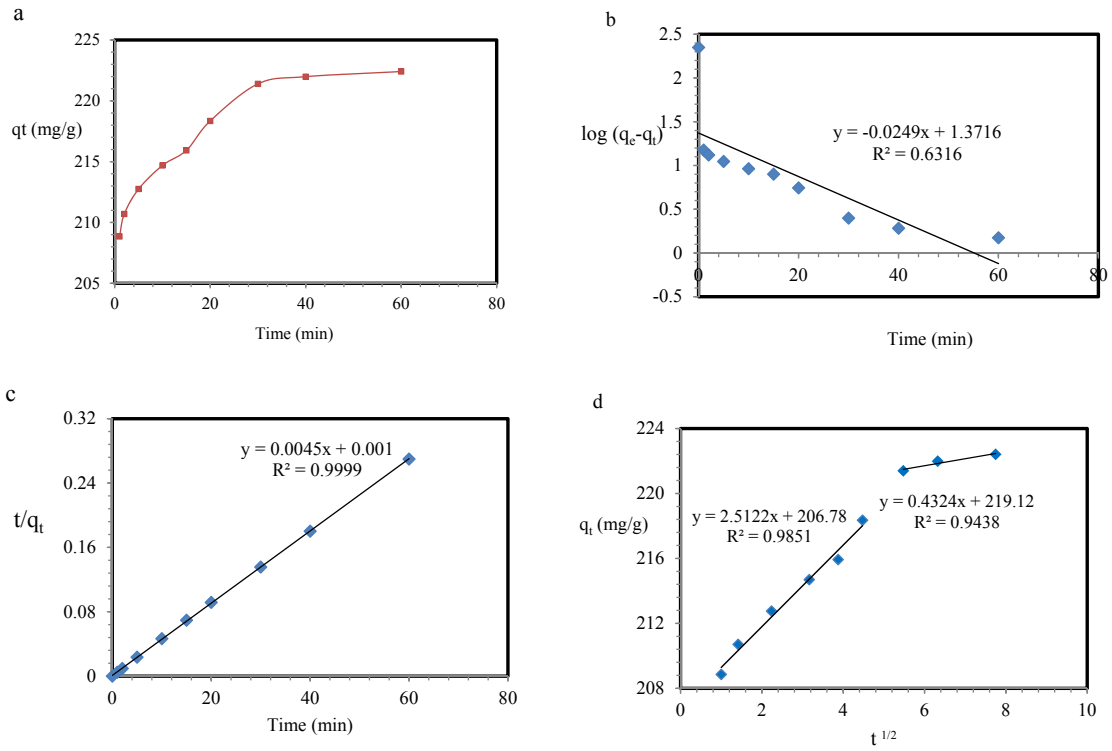

Fig. 6. (a) Effect of contact time on the removal of MB onto Fe_3O_4/AC nanocomposite (b) Plot of pseudo-first-order kinetic, (c) plot of pseudo-second-order kinetic and (d) plot of intra-particle diffusion model.

Isotherm study

The aim of this part is to study of equilibrium relationship between adsorbate and adsorbent. In the other way, isotherm models can describe the correlation between the amount of adsorbate adsorbed on the surface of adsorbent and the amount of adsorbate remained in solution [57]. This relationship was investigated by Langmuir, Freundlich, and Dubinin-Radushkevich isotherm models.

The Langmuir isotherm [11] is based on monolayer adsorption on the surface of the adsorbent. According to this model, there is no interaction between adsorbate ions and all adsorption active sites are energetic uniform. The linear form of the model is:

$$\frac{C_e}{q_e} = \frac{C_e}{q_m} + \frac{1}{q_m b} \quad (9)$$

In this formula, q_m (mg/g) is the maximum amount of MB adsorbed at equilibrium and b (L/mg) is the Langmuir constant related to adsorption energy. The values of the Langmuir constants are determined by plotting C_e/q_e versus C_e.

The feasibility of the Langmuir isotherm model was investigated by the R_L factor (the dimensional factor) [40]. Based on this factor, the adsorption process is favorable since the R_L values in the range of $0 < R_L < 1$.

$$R_L = \frac{1}{1 + bC_o} \quad (10)$$

The Freundlich isotherm [58] is based on multilayer adsorption on the surface of the adsorbent. In this model, the adsorption process occurs by using the non-uniform distribution of adsorption heat and affinities over the heterogeneous surface. The linear form of the model is:

$$\log q_e = \log k_f + \frac{1}{n} \log C_e \quad (11)$$

In this formula, k_f ((mg/g).(L/mg)$^{1/n}$) indicates the adsorption capacity and n indicates the adsorption intensity. The values of the Freundlich constants are determined by plotting log q_e versus log C_e.

The Dubinin–Radushkevich isotherm [46] applies to determine the adsorption type onto a heterogeneous surface. The linear form of the model is:

$$\ln q_e = \ln Q_m - k_D \varepsilon^2 \quad (12)$$

In this formula, Q_m (mmol/g) is the theoretical adsorption capacity, k_D (mol^2/J^2) is the constant related to the adsorption free energy, ε is the polanyi potential (ε =RT ln(1+1/C_e)), R (8.314 J/mol.K) is the gas constant and T (K) is the absolute temperature. The values of the Dubinin–Radushkevich constants are determined by plotting ln q_e versus ε^2.

The mean free energy of adsorption, as a suitable factor for estimating the type of adsorption process, was calculated using the following equation:

$$E = \frac{1}{\sqrt{2k_D}} \quad (13)$$

The adsorption capacity of Fe_3O_4/AC nanocomposite for MB dye was increased with increasing metal dye concentration (Fig. 7a). Fig. 7 (b-d) shows the plots of the Langmuir, Freundlich and Dubinin-Radushkevich isotherms and obtained results are listed in Table 6. By comparing

Table 6. The adsorption isotherms of MB dye

Model	Parameter	Value
Langmuir	b (L/mg)	0.419
	q_m (mg/g)	384.6
	R^2	0.982
	R_L	0.087-0.035
Freundlich	k_f ((mg/g).(L/mg)$^{1/n}$)	121.8
	n	2.193
	1/n	0.455
	R^2	0.934
Dubinin-Radushkevich	k_D (mol^2/J^2)	0.003
	Q_m(mmol/g)	8.944
	E (kJ/mol)	12.5
	R^2	0.942

the values of correlation coefficient R^2 of three isotherms, it is seen that the Langmuir isotherm has the highest value of correlation coefficient (0.982). This means that the equilibrium adsorption data for MB removal fit well to the Langmuir isotherm. In addition, the values of R_L are in the range of 0.087-0.035, which mentioned that the adsorption of MB onto Fe_3O_4/AC nanocomposite is favorable under the conditions selected in this research. Although the value of the correlation coefficient for the Freundlich isotherm is lower as compared to the Langmuir isotherm, but the value of n is higher than 1 (2.193) representing a favorable adsorption. The calculated value of E for the Dubinin–Radushkevich isotherm falls between 8.0 and 16.0 kJ/mol. Thus MB is chemically adsorbed by Fe_3O_4/AC nanocomposite [10]. The maximum adsorption capacity (q_m) of MB adsorption was found to be 384.6 mg/g according to the Langmuir isotherm. According to these results, the Langmuir isotherm best represents the experimental data. In the other words, adsorption of MB onto the surface of adsorbent is monolayer and homogeneous. The Langmuir maximum adsorption capacities of the various adsorbents along with Fe_3O_4/AC nanocomposite are presented in Table 7 [4, 5, 7,

Table 7. Comparison of the maximum adsorption capacities of MB dye onto various adsorbents

Adsorbent	q_m (mg/g)	Reference
Wood waste activated carbon	4.937	[4]
Walnut wood activated carbon	18.51	[5]
Peanut stick activated carbon	2.54	[7]
Albizia lebbeck seed pods Activated carbon	328.3	[13]
Bone charcoal	5	[59]
Fe_3O_4 NPs	45.40	[60]
Gold nanoparticles loaded on activated carbon	185.1	[61]
Calcium alginate-bentonite-activated carbon	994.06	[62]
Cu@ Mn-ZnS-NPs-activated carbon	72.93	[63]
nano-porous modified Na-bentonite	294	[64]
Fe_3O_4/AC nanocomposite	384.6	This study

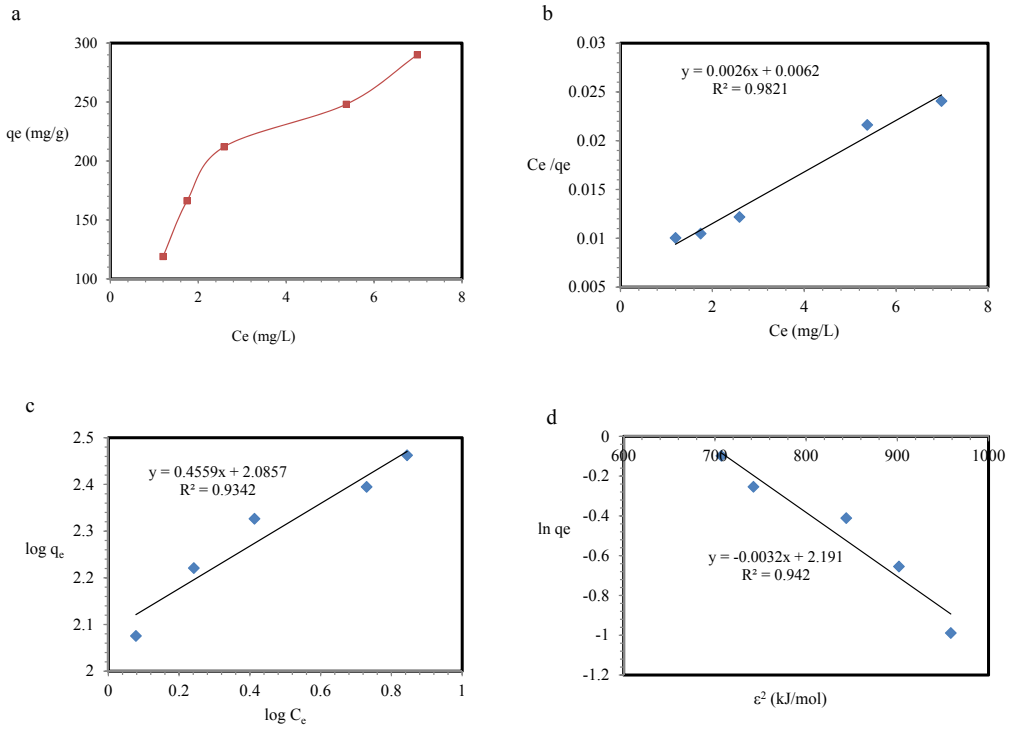

Fig. 7. (a) Effect of initial concentration on the removal of MB onto Fe_3O_4/AC nanocomposite (b) plot of Langmuir isotherm, (c) plot of Freundlich isotherm, and (d) plot of Dubinin-Radushkevich isotherm.

13, 59-64]. The difference in maximum adsorption capacity of the various adsorbents is due to the difference in adsorbent type, activation method and an activation agent. Another factor is the difference in experimental conditions such as pH, temperature, and initial concentration, etc [65].

Thermodynamic study

In this part of the study, the thermodynamic parameters including the change in free energy (ΔG°), enthalpy (ΔH°) and entropy (ΔS°) were determined with equations as follow:

$$\ln K = \frac{\Delta S^{\circ}}{R} - \frac{\Delta H^{\circ}}{RT} \quad (14)$$

$$\Delta G = -RT \ln K \quad (15)$$

In these formulas, T (K) is the absolute temperature and R (8.314 J/mol.K) is the gas constant and K is the equilibrium adsorption constants of the isotherm fits [66].

The values of ΔH° and ΔS° are determined by plotting ln K against 1/T (Fig. 8). Based on the linear plot of Fig. 8 and obtained results in Table 8, it is obvious that the adsorption process onto Fe_3O_4/AC nanocomposite is spontaneous and thermodynamically favorable. The decrease of negative values of ΔG° with the temperature raising means that the adsorption process is more energetically favorable at lower temperatures [67]. The negative value of ΔH° indicates that the adsorption process is exothermic and the positive value of ΔS° indicates the increased randomness at the solid–solution interface.

Adsorption-desorption process

Adsorption-desorption experiments were done three times to check the reusability of Fe_3O_4/AC nanocomposite. Firstly, a solution of HCl (0.1 M) was used to desorb MB ions from Fe_3O_4/AC nanocomposite, and then the nanocomposite was washed with deionized water to reach neutral pH. After three cycles of adsorption-desorption, the removal efficiency of MB dye is shown in Fig. 9. As can be seen in Fig. 9, Fe_3O_4/AC nanocomposite has a potential to be used repeatedly at least for three adsorption-desorption cycles with an insignificant decrease in its removal efficiency.

CONCLUSIONS

In this study Fe_3O_4/AC nanocomposite, a new activated carbon modified iron oxide magnetic nanoparticle was synthesized by microwave assisted and characterized. We used the Taguchi design of experiment to find the best conditions for the removal of cationic dye from solution. Based

Table 8. Thermodynamic parameters for the adsorption of MB dye

ΔH° (kJ/mol)	ΔS° (kJ/mol.K)	ΔG° (kJ/mol)		
		298 K	318 K	333 K
-4.174	0.065	-23.65	-24.98	-25.94

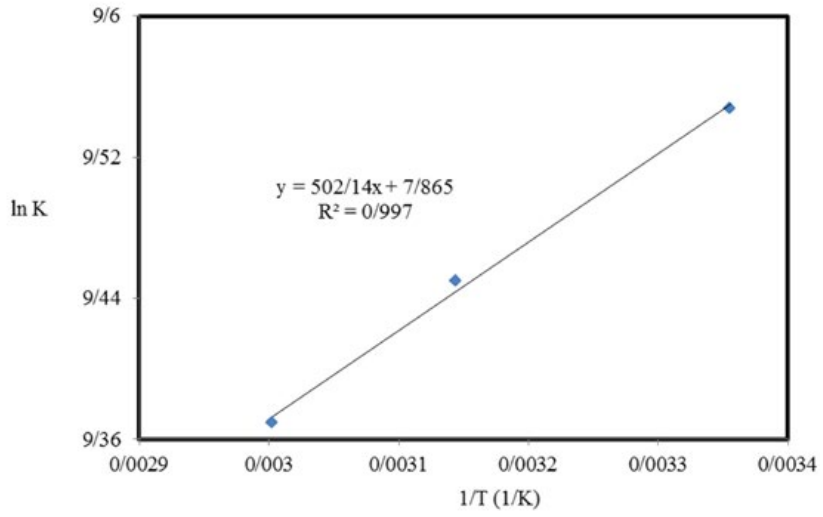

Fig. 8. (a) Plot of log K versus 1/T for sorption of MB onto Fe_3O_4/AC nanocomposite

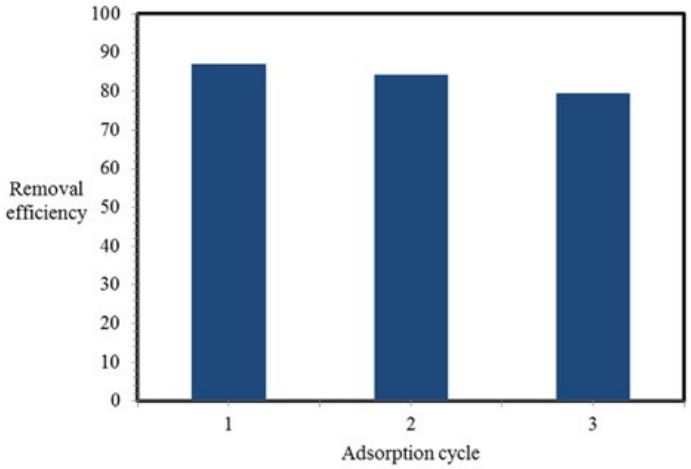

Fig. 9. Adsorption-desorption process

on S/N ratios, the optimum process conditions were pH 7, Fe_3O_4/AC nanocomposite dose 0.03 g, contact time 30 min, initial MB concentration 25 mg/L and temperature 298 K. According to ANOVA results, the influence of the controllable factors in descending order is pH > adsorbent dose > temperature > initial dye concentration > contact time. The kinetics of MB adsorption on Fe_3O_4/AC nanocomposite follows the pseudo-second-order model. The equilibrium data followed the Langmuir isotherm with an adsorption maximum of 384.6 mg/g. This nanocomposite was effectively used for the removal of methylene blue (MB) dye from the aqueous solution.

ACKNOWLEDGMENTS

The authors greatly acknowledgment the financial support from Young Researchers and Elite Club, Arak Branch, Islamic Azad University, Arak, Iran (No. 96066).

CONFLICTS OF INTEREST

The authors declare that there are no conflicts of interest regarding the publication of this manuscript.

REFERENCES

1. Semeraro P, Rizzi V, Fini P, Matera S, Cosma P, Franco E, et al. Interaction between industrial textile dyes and cyclodextrins. Dyes and Pigments. 2015;119:84-94.
2. Agarwal S, Gupta VK, Ghasemi M, Azimi-Amin J. Peganum harmala -L Seeds adsorbent for the rapid removal of noxious brilliant green dyes from aqueous phase. Journal of Molecular Liquids. 2017;231:296-305.
3. Zhang Y-R, Shen S-L, Wang S-Q, Huang J, Su P, Wang Q-R, et al. A dual function magnetic nanomaterial modified with lysine for removal of organic dyes from water solution. Chemical Engineering Journal. 2014;239:250-6.
4. Ghaedi M, Kokhdan SN. Removal of methylene blue from aqueous solution by wood millet carbon optimization using response surface methodology. Spectrochimica Acta Part A: Molecular and Biomolecular Spectroscopy. 2015;136:141-8.
5. Ghaedi M, Mazaheri H, Khodadoust S, Hajati S, Purkait MK. Application of central composite design for simultaneous removal of methylene blue and Pb2+ ions by walnut wood activated carbon. Spectrochimica Acta Part A: Molecular and Biomolecular Spectroscopy. 2015;135:479-90.
6. Ghaedi M, Ghazanfarkhani MD, Khodadoust S, Sohrabi N, Oftade M. Acceleration of methylene blue adsorption onto activated carbon prepared from dross licorice by ultrasonic: Equilibrium, kinetic and thermodynamic studies. Journal of Industrial and Engineering Chemistry. 2014;20(4):2548-60.
7. Ghaedi M, Nasab AG, Khodadoust S, Rajabi M, Azizian S. Application of activated carbon as adsorbents for efficient removal of methylene blue: Kinetics and equilibrium study. Journal of Industrial and Engineering Chemistry. 2014;20(4):2317-24.
8. Gupta VK, Kumar R, Nayak A, Saleh TA, Barakat MA. Adsorptive removal of dyes from aqueous solution onto carbon nanotubes: A review. Advances in Colloid and Interface Science. 2013;193-194:24-34.
9. Mittal A, Mittal J, Malviya A, Kaur D, Gupta VK. Adsorption of hazardous dye crystal violet from wastewater by waste materials. Journal of Colloid and Interface Science. 2010;343(2):463-73.
10. Ghasemi M, Ghasemi N, Zahedi G, Alwi SRW, Goodarzi M, Javadian H. Kinetic and equilibrium study of Ni(II) sorption from aqueous solutions onto Peganum harmala-L. International Journal of Environmental Science and Technology. 2014;11(7):1835-44.
11. Ghasemi M, Naushad M, Ghasemi N, Khosravi-fard Y. A novel agricultural waste based adsorbent for the removal of Pb(II) from aqueous solution: Kinetics, equilibrium and thermodynamic studies. Journal of Industrial and Engineering Chemistry. 2014;20(2):454-61.
12. Ding Z, Hu X, Zimmerman AR, Gao B. Sorption and cosorption of lead (II) and methylene blue on chemically modified biomass. Bioresource Technology. 2014;167:569-73.

13. Ahmed MJ, Theydan SK. Optimization of microwave preparation conditions for activated carbon from Albizia lebbeck seed pods for methylene blue dye adsorption. Journal of Analytical and Applied Pyrolysis. 2014;105:199-208.
14. Omri A, Benzina M, Ammar N. Preparation, modification and industrial application of activated carbon from almond shell. Journal of Industrial and Engineering Chemistry. 2013;19(6):2092-9.
15. Zhao Y, Xia Y, Yang H, Wang Y, Zhao M. Synthesis of glutamic acid-modified magnetic corn straw: equilibrium and kinetic studies on methylene blue adsorption. Desalination and Water Treatment. 2013;52(1-3):199-207.
16. Ahmadzadeh Tofighy M, Mohammadi T. Methylene blue adsorption onto granular activated carbon prepared from Harmal seeds residue. Desalination and Water Treatment. 2013;52(13-15):2643-53.
17. Krishni RR, Foo KY, Hameed BH. Adsorption of methylene blue onto papaya leaves: comparison of linear and nonlinear isotherm analysis. Desalination and Water Treatment. 2013;52(34-36):6712-9.
18. Tran HN, Viet PV, Chao H-P. Surfactant modified zeolite as amphiphilic and dual-electronic adsorbent for removal of cationic and oxyanionic metal ions and organic compounds. Ecotoxicology and Environmental Safety. 2018;147:55-63.
19. Safarik I, Angelova R, Baldikova E, Pospiskova K, Safarikova M. Leptothrix sp. sheaths modified with iron oxide particles: Magnetically responsive, high aspect ratio functional material. Materials Science and Engineering: C. 2017;71:1342-6.
20. Cheng S, Zhang L, Ma A, Xia H, Peng J, Li C, et al. Comparison of activated carbon and iron/cerium modified activated carbon to remove methylene blue from wastewater. Journal of Environmental Sciences. 2018;65:92-102.
21. Al-Othman ZA, Ali R, Naushad M. Hexavalent chromium removal from aqueous medium by activated carbon prepared from peanut shell: Adsorption kinetics, equilibrium and thermodynamic studies. Chemical Engineering Journal. 2012;184:238-47.
22. Pan J, Zou X, Wang X, Guan W, Li C, Yan Y, et al. Adsorptive removal of 2,4-didichlorophenol and 2,6-didichlorophenol from aqueous solution by β-cyclodextrin/attapulgite composites: Equilibrium, kinetics and thermodynamics. Chemical Engineering Journal. 2011;166(1):40-8.
23. Zhou S, Xue A, Zhang Y, Li M, Li K, Zhao Y, et al. Novel polyamidoamine dendrimer-functionalized palygorskite adsorbents with high adsorption capacity for Pb2+ and reactive dyes. Applied Clay Science. 2015;107:220-9.
24. Sun X, Yang L, Li Q, Zhao J, Li X, Wang X, et al. Amino-functionalized magnetic cellulose nanocomposite as adsorbent for removal of Cr(VI): Synthesis and adsorption studies. Chemical Engineering Journal. 2014;241:175-83.
25. Xin X, Wei Q, Yang J, Yan L, Feng R, Chen G, et al. Highly efficient removal of heavy metal ions by amine-functionalized mesoporous Fe3O4 nanoparticles. Chemical Engineering Journal. 2012;184:132-40.
26. Wong KT, Eu NC, Ibrahim S, Kim H, Yoon Y, Jang M. Recyclable magnetite-loaded palm shell-waste based activated carbon for the effective removal of methylene blue from aqueous solution. Journal of Cleaner Production. 2016;115:337-42.
27. Osouli-Bostanabad K, Hosseinzade E, Kianvash A, Entezami A. Modified nano-magnetite coated carbon fibers magnetic and microwave properties. Applied Surface Science. 2015;356:1086-95.
28. Hernández-Hernández AA, Álvarez-Romero GA, Castañeda-Ovando A, Mendoza-Tolentino Y, Contreras-López E, Galán-Vidal CA, et al. Optimization of microwave-solvothermal synthesis of Fe3O4 nanoparticles. Coating, modification, and characterization. Materials Chemistry and Physics. 2018;205:113-9.
29. S S, P SK, A S, P SR, C R. Computation of adsorption parameters for the removal of dye from wastewater by microwave assisted sawdust: Theoretical and experimental analysis. Environmental Toxicology and Pharmacology. 2017;50:45-57.
30. Bazgir S and Farhadi S (2017) Microwave-assisted rapid synthesis of Co3O4 nanorods from CoC2O4.2H2O nanorods and its application in photocatalytic degradation of methylene blue under visible light irradiation, Int. J. Nano Dimens. 8 (4): 284-297.
31. Rahimmalek M, Mirzakhani M, Pirbalouti AG. Essential oil variation among 21 wild myrtle (Myrtus communis L.) populations collected from different geographical regions in Iran. Industrial Crops and Products. 2013;51:328-33.
32. Kazemi SY, Biparva P, Ashtiani E. Cerastoderma lamarcki shell as a natural, low cost and new adsorbent to removal of dye pollutant from aqueous solutions: Equilibrium and kinetic studies. Ecological Engineering. 2016;88:82-9.
33. Rahmani M, Kaykhaii M, Sasani M. Application of Taguchi L16 design method for comparative study of ability of 3A zeolite in removal of Rhodamine B and Malachite green from environmental water samples. Spectrochimica Acta Part A: Molecular and Biomolecular Spectroscopy. 2018;188:164-9.
34. Demirbas E, Kobya M, Oncel S, Sencan S (2002) Removal of Ni(II) from aqueous solution by adsorption onto hazelnut shell activated carbon: equilibrium studies, Bioresource Technology 84: 291–293.
35. Yen HY, Li JY. Process optimization for Ni(II) removal from wastewater by calcined oyster shell powders using Taguchi method. Journal of Environmental Management. 2015;161:344-9.
36. Engin AB, Özdemir Ö, Turan M, Turan AZ. Color removal from textile dyebath effluents in a zeolite fixed bed reactor: Determination of optimum process conditions using Taguchi method. Journal of Hazardous Materials. 2008;159(2-3):348-53.
37. Asgari G, Feradmal J, Poormohammadi A, Sadrnourmohamadi M, Akbari S. Taguchi optimization for the removal of high concentrations of phenol from saline wastewater using electro-Fenton process. Desalination and Water Treatment. 2016;57(56):27331-8.
38. Hu J-P, Liu R-L, Liu J-S, Zhao S-Y, Lin X, Lai W-L. Thermodynamic behavior of adsorption of copper (II) ion on Wuyi Rock Tea Dreg. Desalination and Water Treatment. 2013;52(37-39):7196-204.
39. Khataee A, Kayan B, Kalderis D, Karimi A, Akay S, Konsolakis M. Ultrasound-assisted removal of Acid Red 17 using nanosized Fe 3 O 4 -loaded coffee waste hydrochar. Ultrasonics Sonochemistry. 2017;35:72-80.
40. Ghasemi M, Zeinaly Khosroshahy M, Bavand Abbasabadi A, Ghasemi N, Javadian H, Fattahi M. Microwave-assisted functionalization of Rosa Canina-L fruits activated carbon with tetraethylenepentamine and its adsorption behavior toward Ni(II) in aqueous solution: Kinetic, equilibrium and thermodynamic studies. Powder Technology. 2015;274:362-71.

41. Varala S, Kumari A, Dharanija B, Bhargava SK, Parthasarathy R, Satyavathi B. Removal of thorium (IV) from aqueous solutions by deoiled karanja seed cake: Optimization using Taguchi method, equilibrium, kinetic and thermodynamic studies. Journal of Environmental Chemical Engineering. 2016;4(1):405-17.
42. Ge F, Li M-M, Ye H, Zhao B-X. Effective removal of heavy metal ions Cd2+, Zn2+, Pb2+, Cu2+ from aqueous solution by polymer-modified magnetic nanoparticles. Journal of Hazardous Materials. 2012;211-212:366-72.
43. Shakib F, Dadvand Koohi A, Kamran Pirzaman A. Adsorption of methylene blue by using novel chitosan-g-itaconic acid/bentonite nanocomposite – equilibrium and kinetic study. Water Science and Technology. 2017;75(8):1932-43.
44. Bardajee GR, Hooshyar Z, Shahidi FE. Synthesis and characterization of a novel Schiff-base/SBA-15 nanoadsorbent for removal of methylene blue from aqueous solutions. International Journal of Environmental Science and Technology. 2014;12(5):1737-48.
45. Jafari S, Zhao F, Zhao D, Lahtinen M, Bhatnagar A, Sillanpää M. A comparative study for the removal of methylene blue dye by N and S modified TiO2 adsorbents. Journal of Molecular Liquids. 2015;207:90-8.
46. Ghasemi M, Naushad M, Ghasemi N, Khosravi-fard Y. Adsorption of Pb(II) from aqueous solution using new adsorbents prepared from agricultural waste: Adsorption isotherm and kinetic studies. Journal of Industrial and Engineering Chemistry. 2014;20(4):2193-9.
47. Manna S, Roy D, Saha P, Gopakumar D, Thomas S. Rapid methylene blue adsorption using modified lignocellulosic materials. Process Safety and Environmental Protection. 2017;107:346-56.
48. Shao H, Li Y, Zheng L, Chen T, Liu J. Removal of methylene blue by chemically modified defatted brown algae Laminaria japonica. Journal of the Taiwan Institute of Chemical Engineers. 2017;80:525-32.
49. Davoodi S, Marahel F, Ghaedi M, Roosta M, Hekmati Jah A. Tin oxide nanoparticles loaded on activated carbon as adsorbent for removal of Murexide. Desalination and Water Treatment. 2013;52(37-39):7282-92.
50. Unuabonah EI, Adie GU, Onah LO, Adeyemi OG. Multistage optimization of the adsorption of methylene blue dye onto defatted Carica papaya seeds. Chemical Engineering Journal. 2009;155(3):567-79.
51. Bouaziz F, Koubaa M, Kallel F, Chaari F, Driss D, Ghorbel RE, et al. Efficiency of almond gum as a low-cost adsorbent for methylene blue dye removal from aqueous solutions. Industrial Crops and Products. 2015;74:903-11.
52. Gupta VK, Pathania D, Agarwal S, Sharma S. De-coloration of hazardous dye from water system using chemically modified Ficus carica adsorbent. Journal of Molecular Liquids. 2012;174:86-94.
53. Yunessnia lehi A, Akbari A. Novel membrane adsorbents prepared by waste fibers of mechanized carpet for Persian Orange X removal. Environmental Nanotechnology, Monitoring & Management. 2017;8:209-18.
54. Aflaki Jalali M, Dadvand Koohi A, Sheykhan M. Experimental study of the removal of copper ions using hydrogels of xanthan, 2-acrylamido-2-methyl-1-propane sulfonic acid, montmorillonite: Kinetic and equilibrium study. Carbohydrate Polymers. 2016;142:124-32.
55. Asgari G, Roshani B, Ghanizadeh G. The investigation of kinetic and isotherm of fluoride adsorption onto functionalize pumice stone. Journal of Hazardous Materials. 2012;217-218:123-32.
56. Tian G, Wang W, Kang Y, Wang A. Palygorskite in sodium sulphide solution via hydrothermal process for enhanced methylene blue adsorption. Journal of the Taiwan Institute of Chemical Engineers. 2016;58:417-23.
57. Reddy P.M.K, Verma P, Subrahmanyam C (2016) Bio-waste derived adsorbent material form ethylene blue adsorption, Journal of the Taiwan Institute of Chemical Engineers 58: 500–508.
58. Nazari G, Abolghasemi H, Esmaieli M. Batch adsorption of cephalexin antibiotic from aqueous solution by walnut shell-based activated carbon. Journal of the Taiwan Institute of Chemical Engineers. 2016;58:357-65.
59. Ghanizadeh G, Asgari G. Adsorption kinetics and isotherm of methylene blue and its removal from aqueous solution using bone charcoal. Reaction Kinetics, Mechanisms and Catalysis. 2010;102(1):127-42.
60. Ghaedi M, Hajjati S, Mahmudi Z, Tyagi I, Agarwal S, Maity A, et al. Modeling of competitive ultrasonic assisted removal of the dyes – Methylene blue and Safranin-O using Fe3O4 nanoparticles. Chemical Engineering Journal. 2015;268:28-37.
61. Roosta M, Ghaedi M, Daneshfar A, Sahraei R, Asghari A. Optimization of the ultrasonic assisted removal of methylene blue by gold nanoparticles loaded on activated carbon using experimental design methodology. Ultrasonics Sonochemistry. 2014;21(1):242-52.
62. Benhouria A, Islam MA, Zaghouane-Boudiaf H, Boutahala M, Hameed BH. Calcium alginate–bentonite–activated carbon composite beads as highly effective adsorbent for methylene blue. Chemical Engineering Journal. 2015;270:621-30.
63. Dastkhoon M, Ghaedi M, Asfaram A, Goudarzi A, Mohammadi SM, Wang S. Improved adsorption performance of nanostructured composite by ultrasonic wave: Optimization through response surface methodology, isotherm and kinetic studies. Ultrasonics Sonochemistry. 2017;37:94-105.
64. Moradi N, Salem S, Salem A. Optimizing adsorption of blue pigment from wastewater by nano-porous modified Na-bentonite using spectrophotometry based on response surface method. Spectrochimica Acta Part A: Molecular and Biomolecular Spectroscopy. 2018;193:54-62.
65. Pawar RR, Lalhmunsiama, Bajaj HC, Lee S-M. Activated bentonite as a low-cost adsorbent for the removal of Cu(II) and Pb(II) from aqueous solutions: Batch and column studies. Journal of Industrial and Engineering Chemistry. 2016;34:213-23.
66. Alqadami AA, Naushad M, Abdalla MA, Khan MR, Alothman ZA. Adsorptive Removal of Toxic Dye Using Fe3O4–TSC Nanocomposite: Equilibrium, Kinetic, and Thermodynamic Studies. Journal of Chemical & Engineering Data. 2016;61(11):3806-13.
67. Petrović M, Šoštarić T, Stojanović M, Milojković J, Mihajlović M, Stanojević M, et al. Removal of Pb 2+ ions by raw corn silk (Zea mays L.) as a novel biosorbent. Journal of the Taiwan Institute of Chemical Engineers. 2016;58:407-16.